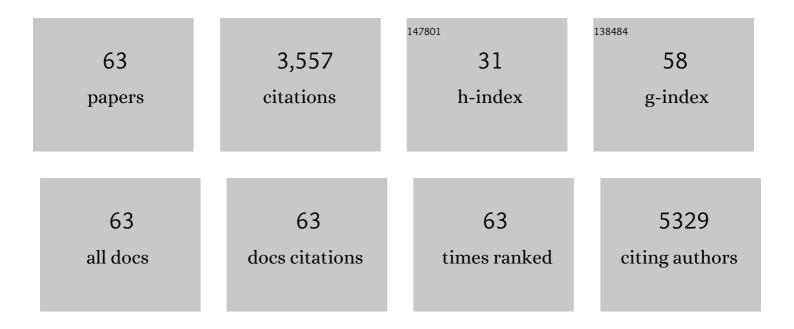
Kemin Tan

List of Publications by Year in descending order

Source: https://exaly.com/author-pdf/4312709/publications.pdf Version: 2024-02-01



KEMIN TAN

#	Article	IF	CITATIONS
1	Pre–T cell receptors topologically sample self-ligands during thymocyte β-selection. Science, 2021, 371, 181-185.	12.6	25
2	Tying the knot in the tetrahydrofolate (THF) riboswitch: A molecular basis for gene regulation. Journal of Structural Biology, 2021, 213, 107703.	2.8	7
3	Sensor Domain of Histidine Kinase VxrA of Vibrio cholerae: Hairpin-Swapped Dimer and Its Conformational Change. Journal of Bacteriology, 2021, 203, .	2.2	4
4	Masitinib is a broad coronavirus 3CL inhibitor that blocks replication of SARS-CoV-2. Science, 2021, 373, 931-936.	12.6	173
5	Structural and biochemical insights into CRISPR RNA processing by the Cas5c ribonuclease SMU1763 from Streptococcus mutans. Journal of Biological Chemistry, 2021, 297, 101251.	3.4	2
6	Structural and functional characterization of three Type B and C chloramphenicol acetyltransferases from <i>Vibrio</i> species. Protein Science, 2020, 29, 695-710.	7.6	12
7	FMN riboswitch aptamer symmetry facilitates conformational switching through mutually exclusive coaxial stacking configurations. Journal of Structural Biology: X, 2020, 4, 100035.	1.3	15
8	Mechanistic insights from structure of Mycobacterium smegmatis topoisomerase I with ssDNA bound to both N- and C-terminal domains. Nucleic Acids Research, 2020, 48, 4448-4462.	14.5	12
9	Structures of teixobactin-producing nonribosomal peptide synthetase condensation and adenylation domains. Current Research in Structural Biology, 2020, 2, 14-24.	2.2	18
10	Room-temperature X-ray crystallography reveals the oxidation and reactivity of cysteine residues in SARS-CoV-2 3CL M ^{pro} : insights into enzyme mechanism and drug design. IUCrJ, 2020, 7, 1028-1035.	2.2	49
11	Structural analysis of free and liganded forms of the Fab fragment of a high-affinity anti-cocaine antibody, h2E2. Acta Crystallographica Section F, Structural Biology Communications, 2019, 75, 697-706.	0.8	7
12	Incorporation of isotopic, fluorescent, and heavy-atom-modified nucleotides into RNAs by position-selective labeling of RNA. Nature Protocols, 2018, 13, 987-1005.	12.0	27
13	Interaction of antidiabetic αâ€glucosidase inhibitors and gut bacteria αâ€glucosidase. Protein Science, 2018, 27, 1498-1508.	7.6	37
14	Functional Profiling and Crystal Structures of Isothiocyanate Hydrolases Found in Gut-Associated and Plant-Pathogenic Bacteria. Applied and Environmental Microbiology, 2018, 84, .	3.1	16
15	Investigating mycobacterial topoisomerase I mechanism from the analysis of metal and DNA substrate interactions at the active site. Nucleic Acids Research, 2018, 46, 7296-7308.	14.5	23
16	Insights into PGâ€binding, conformational change, and dimerization of the OmpA Câ€ŧerminal domains from Salmonella enterica serovar Typhimurium and Borrelia burgdorferi. Protein Science, 2017, 26, 1738-1748.	7.6	8
17	Structure of thrombospondin type 3 repeats in bacterial outer membrane protein A reveals its intra-repeat disulfide bond-dependent calcium-binding capability. Cell Calcium, 2017, 66, 78-89.	2.4	7
18	Crystal Structures of SgcE6 and SgcC, the Two-Component Monooxygenase That Catalyzes Hydroxylation of a Carrier Protein-Tethered Substrate during the Biosynthesis of the Enediyne Antitumor Antibiotic C-1027 in <i>Streptomyces globisporus</i> . Biochemistry, 2016, 55, 5142-5154.	2.5	18

Κεμιν Ταν

#	Article	IF	CITATIONS
19	Structure and function of human Naa60 (NatF), a Golgi-localized bi-functional acetyltransferase. Scientific Reports, 2016, 6, 31425.	3.3	25
20	Insights from the Structure of Mycobacterium tuberculosis Topoisomerase I with a Novel Protein Fold. Journal of Molecular Biology, 2016, 428, 182-193.	4.2	36
21	EsxB, a secreted protein from <scp><i>B</i></scp> <i>acillus anthracis</i> forms two distinct helical bundles. Protein Science, 2015, 24, 1389-1400.	7.6	12
22	Structural basis for suppression of hypernegative DNA supercoiling by <i>E. coli</i> topoisomerase I. Nucleic Acids Research, 2015, 43, 11031-11046.	14.5	52
23	<i>In situ</i> X-ray data collection and structure phasing of protein crystals at Structural Biology Center 19-ID. Journal of Synchrotron Radiation, 2015, 22, 1386-1395.	2.4	8
24	Functional Diversity of Haloacid Dehalogenase Superfamily Phosphatases from Saccharomyces cerevisiae. Journal of Biological Chemistry, 2015, 290, 18678-18698.	3.4	70
25	Sensor Domain of Histidine Kinase KinB of Pseudomonas. Journal of Biological Chemistry, 2014, 289, 12232-12244.	3.4	11
26	GH1-family 6-P-Î ² -glucosidases from human microbiome lactic acid bacteria. Acta Crystallographica Section D: Biological Crystallography, 2013, 69, 451-463.	2.5	19
27	Structural and functional characterization of solute binding proteins for aromatic compounds derived from lignin: <i>p</i> -Coumaric acid and related aromatic acids. Proteins: Structure, Function and Bioinformatics, 2013, 81, 1709-1726.	2.6	21
28	Biochemical and Structural Studies of Uncharacterized Protein PA0743 from Pseudomonas aeruginosa Revealed NAD+-dependent l-Serine Dehydrogenase. Journal of Biological Chemistry, 2012, 287, 1874-1883.	3.4	23
29	The crystal structures of the α-subunit of the α2β2 tetrameric Glycyl-tRNA synthetase. Journal of Structural and Functional Genomics, 2012, 13, 233-239.	1.2	11
30	Bifidobacterium longum subsp. infantis ATCC 15697 α-Fucosidases Are Active on Fucosylated Human Milk Oligosaccharides. Applied and Environmental Microbiology, 2012, 78, 795-803.	3.1	204
31	A conformational switch controls cell wallâ€remodelling enzymes required for bacterial cell division. Molecular Microbiology, 2012, 85, 768-781.	2.5	98
32	The structure of the Ca2+-binding, glycosylated F-spondin domain of F-spondin - A C2-domain variant in an extracellular matrix protein. BMC Structural Biology, 2011, 11, 22.	2.3	9
33	Cleavable C-terminal His-tag vectors for structure determination. Journal of Structural and Functional Genomics, 2010, 11, 31-39.	1.2	38
34	N. meningitidis1681 is a member of the FinO family of RNA chaperones. RNA Biology, 2010, 7, 812-819.	3.1	28
35	Novel αâ€glucosidase from human gut microbiome: substrate specificities and their switch. FASEB Journal, 2010, 24, 3939-3949.	0.5	49
36	The crystal structure of the signature domain of cartilage oligomeric matrix protein: implications for collagen, glycosaminoglycan and integrin binding. FASEB Journal, 2009, 23, 2490-2501.	0.5	63

Kemin Tan

#	Article	IF	CITATIONS
37	The Mannitol Operon Repressor MtlR Belongs to a New Class of Transcription Regulators in Bacteria. Journal of Biological Chemistry, 2009, 284, 36670-36679.	3.4	14
38	The interaction of Thrombospondins with extracellular matrix proteins. Journal of Cell Communication and Signaling, 2009, 3, 177-187.	3.4	95
39	Structure and electrostatic property of cytoplasmic domain of ZntB transporter. Protein Science, 2009, 18, 2043-2052.	7.6	15
40	Large-scale evaluation of protein reductive methylation for improving protein crystallization. Nature Methods, 2008, 5, 853-854.	19.0	81
41	Structures of open (R) and close (T) states of prephenate dehydratase (PDT)—Implication of allosteric regulation by I-phenylalanine. Journal of Structural Biology, 2008, 162, 94-107.	2.8	34
42	The Crystal Structure of the Heparin-Binding Reelin-N Domain of F-Spondin. Journal of Molecular Biology, 2008, 381, 1213-1223.	4.2	21
43	Heparin-induced cis- and trans-Dimerization Modes of the Thrombospondin-1 N-terminal Domain. Journal of Biological Chemistry, 2008, 283, 3932-3941.	3.4	33
44	Structure of the influenza virus A H5N1 nucleoprotein: implications for RNA binding, oligomerization, and vaccine design. FASEB Journal, 2008, 22, 3638-3647.	0.5	186
45	In situ proteolysis for protein crystallization and structure determination. Nature Methods, 2007, 4, 1019-1021.	19.0	197
46	The Structures of the Thrombospondin-1 N-Terminal Domain and Its Complex with a Synthetic Pentameric Heparin. Structure, 2006, 14, 33-42.	3.3	80
47	CD8αβ Has Two Distinct Binding Modes of Interaction with Peptide-Major Histocompatibility Complex Class I. Journal of Biological Chemistry, 2006, 281, 28090-28096.	3.4	13
48	Structural and Mutational Analyses of a CD8αβ Heterodimer and Comparison with the CD8αα Homodimer. Immunity, 2005, 23, 661-671.	14.3	39
49	Crystal structure of the TSP-1 type 1 repeats. Journal of Cell Biology, 2002, 159, 373-382.	5.2	249
50	Crystal structure of murine sCEACAM1a[1,4]: a coronavirus receptor in the CEA family. EMBO Journal, 2002, 21, 2076-2086.	7.8	102
51	The Role of α and β Chains in Ligand Recognition by β7 Integrins. Journal of Biological Chemistry, 2000, 275, 25652-25664.	3.4	36
52	Molecular Basis for Leukocyte Integrin αEβ7 Adhesion to Epithelial (E)-Cadherin. Journal of Experimental Medicine, 2000, 191, 1555-1567.	8.5	56
53	Mutational analysis of MAdCAM-1/α4β7 interactions reveals significant binding determinants in both the first and second immunoglobulin domains. Cell Adhesion and Communication, 1999, 7, 167-181.	1.7	20
54	The Crystal Structure of a T Cell Receptor in Complex with Peptide and MHC Class II. Science, 1999, 286, 1913-1921.	12.6	376

Kemin Tan

#	Article	IF	CITATIONS
55	Structure of a Heterophilic Adhesion Complex between the Human CD2 and CD58 (LFA-3) Counterreceptors. Cell, 1999, 97, 791-803.	28.9	216
56	The structure of immunoglobulin superfamily domains 1 and 2 of MAdCAM-1 reveals novel features important for integrin recognition. Structure, 1998, 6, 793-801.	3.3	64
57	Structure of Microporous QUI-MnGS-1 and in Situ Studies of Its Formation Using Time-Resolved Synchrotron X-ray Powder Diffraction. Chemistry of Materials, 1998, 10, 1453-1458.	6.7	40
58	Hydrothermal Growth of Single Crystals of TMA-CuGS-2, [C4H12N]6[(Cu0.44Ge0.56S2.23)4(Ge4S8)3] and Their Characterization Using Synchrotron/Imaging Plate Data. Chemistry of Materials, 1996, 8, 448-453.	6.7	71
59	Synthesis of a Novel Two-Dimensional Antimony Sulfide, [C4H10N]2[Sb8S13]·0.15H2O, and Its Structure Solution Using Synchrotron/Imaging Plate Data. Chemistry of Materials, 1996, 8, 493-496.	6.7	39
60	A Novel Antimony Sulfide Templated by Dimethylammonium:  Its Synthesis and Structural Characterization Using Synchrotron/Imaging Plate Data. Chemistry of Materials, 1996, 8, 2510-2515.	6.7	40
61	Novel Two-Dimensional Tin Sulfide Networks: Preparation and Structural Characterization of Sn4S9[(C3H7)4N]2 and Sn4S9[(C3H7)4N] · [(CH3)3NH]. Journal of Solid State Chemistry, 1995, 114, 506-511.	2.9	62
62	Structural Evolution from Tin Sulfide (Selenide) Layered Structures to Novel 3- and 4-Connected Tin Oxy-sulfides. Journal of Solid State Chemistry, 1995, 117, 219-228.	2.9	45
63	Synthesis of a novel open-framework sulfide, CuGe2S5.(C2H5)4N, and its structure solution using synchrotron imaging plate data. Journal of the American Chemical Society, 1995, 117, 7039-7040.	13.7	96